Comparative study of alpha scattering from various nuclei at 130 MeV: Microscopic potentials and coupled channel calculations

Awad A. Ibraheem[a,b,c]
[a]*Research Center for Advanced Materials Science (RCAMS),*
King Khalid University, Abha, 61413, P.O Box 9004, Saudi Arabia,
[b]*Physics Department, King Khalid University, Abha, Saudi Arabia,*
[c]*Physics Department, Al-Azhar University, Assiut Branch, Assiut 71524, Egypt.*

F. Alasmary
Department of Physics, College of Sciences, University of Bisha,Bisha 61922, P.O.Box551,Saudi arabia.

B. Alshahrani
Physics Department, King Khalid University, Abha, Saudi Arabia.

M. Karakoç
Department of Physics, Faculty of Science, Akdeniz University, TR 07070, Antalya, Türkiye.

Sh. Hamada
Physics Department, Faculty of Science, Tanta University, Tanta, Egypt.

M. N. El-Hammamy
PhysicsDepartment, Faculty of Science, Damanhur University, Damanhur, Egypt.

Received 13 June 2023; accepted 23 December 2023

The angular distributions of the elastic and inelastic scattering cross sections of alpha projectiles on different heavy ion target nuclei, including ^{12}C, ^{16}O, ^{24}Mg, ^{28}Si, and ^{40}Ca, at energy of 130 MeV have been studied using two different microscopic real potentials generated by the energy density functional (EDF) theory and single folding cluster model, as well as phenomenological Woods-Saxon potentials. A new parameterization was considered for the first time by EDF, and to make the normalization coefficient tend to unity, it is necessary to consider a correction to the calculated real potential. Coupled channel calculations for various low-lying excited states of the considered targets were performed, and the optimal extracted deformation lengths within the employed models were extracted and compared to previous reported values. The total reaction cross section, as well as the real and imaginary volume integrals, have been studied.

Keywords: Energy density functional; single folding cluster; deformation length parameter.

DOI: https://doi.org/10.31349/RevMexFis.70.031202

1. Introduction

A key tool for understanding nuclear force characteristics in a few body systems is to observe cluster configurations in light nuclei [1]. Clustering in nuclei is a result of the quantum structure of nuclear systems, which allows for correlations between nucleons within the nucleus. This behavior manifests itself in different ways: sometimes as a collection of subsystems with tightly-bounded positions like ^{8}Be [2] and ^{12}C [3], or as clusters that spin away from the core and produce rotational energy spectra when close to doubly-magic closure (*e.g.*, ^{4}He + d/t for ^{6}Li/^{7}Li) [4,5]. Other times, such as in Borromean nuclei like ^{6}He, one neutron's wave function may appear in the 'forbidden zone' and will split into two components if removed—a single neutron and an alpha particle [1]. Further still, there are *alpha* conjugate nuclei (A=*m-alpha*) which exhibit progressive transitions from ground state to complete *m-alpha* release upon excitation energy addition [6-9]. This paper examines such structures by way of scattering reactions.

Alpha-particle scattering from *alpha* conjugate nuclei (*e.g.* ^{12}C, ^{20}Ne, ^{40}Ca, etc.) is of particular interest due to the observation of anomalous large-angle scattering (ALAS) and nuclear rainbow scattering at energies below 50 MeV and above 100 MeV, respectively [10-12]. These two phenomena help in understanding the *alpha*-nucleus potentials in both short-range and surface regions. To explain these events, a uniquely shaped *alpha*-nucleus optical potential must be established [11].

The single folding cluster (SFC) model has been shown to provide a consistent framework for reliably calculating the real *alpha*-nucleus potential. By folding the *alpha-alpha* effective interaction with the *alpha*-cluster density distributions in the colliding nuclei, the SFC model drastically reduces free parameters and gives a solid microscopic foundation for real *alpha*-nucleus potentials. However, there are still some quandaries associated with this approach; normalization of the derived potentials may be necessary and the *alpha*-particle density used in folding could fail to accurately reproduce its observed binding energy -B.E- [13-16]. Therefore, the energy density functional (EDF) method provides another path to accurately ascertain the real part of the *alpha*-nucleus potential by leveraging two nucleons potential. The success of the derived potential depends on how well the (B.E) of the interacting nuclei are produced from their density distribution functions [17,18]. The EDF potential has proven successful at describing low energy scattering data across a multitude of targets without the need for renormalization [18-21], in contrast to high energies. Hence, this route circumvents many of the errors associated with the SFC model.

Adachi *et al.* [22], for example, demonstrated how *alpha*-nucleus interactions using single folding (SF) potentials could yield successful calculations for both elastic and inelastic *alpha* scattering across various excited low lying states in numerous target nuclei at 130 and 386 MeV. Several other reports (e.g. Refs. [23-30]) corroborated this notion as well. El-Azab Farid et al. [13,26] further incorporated *alpha*-cluster structures into the folding model using single-folding cluster (SFC) and double-folding cluster (DFC) models with a suitable *alpha*-*alpha* interaction. Although these theories generated successful outcomes for most heavy ion elastic scattering reactions, a reduction in renormalization factors (between 0.7-0.9) was nonetheless implemented during the process. Subsequently, Abdullah et al. [15,31] devised a SFC approach to accurately assess the differential cross-section of *alpha*-particles on ^{16}O and ^{40,44,48}Ca over a wide variety of incoming energies; alluding to the notion that majority of nucleons take an *alpha*-like clustered form inside target nuclei accompanied by unclustered nucleonic entities. Hence, they were able to formulate a folding potential composed of two separate potentials convolution the *alpha*-cluster density distribution and the nucleonic density distribution. This pioneering technique eliminated the need for renormalization while satisfactorily matching empirical data. Hassanain [32] put this theory to the test when analyzing *alpha*-^{24}Mg and ^{28}Si scattering from 22 to 175 MeV energy levels through the same SFC model. His work yielded positive results, correctly predicting ALAS and rainbow events without requiring renormalization. Awad and Aygun [30] also used SFC, DF, and phenomenological optical models when examining 40, 48 and 54 MeV elastic and inelastic *alpha*-particle scattering from ^{36}Ar - confirming past deformation length values. Lately, Basak et al. [21], used the non-monotonic (NM) EDF-derived potential in analyzing the measured differential cross sections of *alpha* elastic scattering by ^{40}Ca in the energy range of 36.1-42.6 MeV. They reported the well accounted airy structure of the rainbow scattering data by the shallow NM potential. Very recently, Mahmoud [33] studied the elastic scattering of *alpha*-particles from ^{12}C, ^{16}O, ^{20}Ne, ^{24}Mg, ^{28}Si, ^{32}S, and ^{40}Ca at two energies for the majority of the targets, 120 and 130 MeV, utilizing the SFC and the traditional DF model. By using the EDF predicted *alpha*-cluster densities, his results highlighted that an *alpha*-particle's behavior inside a nucleus may differ from its free state which necessitated normalization by a factor of 0.75 for precise computations.

In light of this, the main goal of this research is to demonstrate, for the first time, the efficacy of the various real EDF potentials in describing intermediate energy *alpha* particle scattering data for a variety of targets (^{12}C, ^{16}O, ^{24}Mg, ^{28}Si, and ^{40}Ca) in comparison to the widely used SFC and phenomenological Woods-Saxon (WS) potentials. For this reason, it is essential to examine the consistency of the generated EDF potential in relation to varying target densities. It is necessary to account for EDF corrections to the calculated real part by introducing a normalization coefficient closer to one. In addition to the three real potential forms; EDF, SFC, and WS, the imaginary potential was taken in the usual WS shape. The second objective is to evaluate the success of the employed potentials in determining the deformation length parameter for the investigated targets when scattered inelastically by *alpha* particles. Using coupled channel calculations (CC) with fitted elastic scattering parameters, transition potentials associated with the energy excited states (2_1^+,3_1^-, and 4_1^+) were determined. Additionally, the results are validated by comparing them to previous results. Therefore, it should be noted that this work complements our previous research for various nuclear systems, such as Refs. [30,34].

The paper itself divided into three sections following the introduction: In Sec. 2, we present the theoretical formulation; in Sec 3, we discuss our findings before concluding in Sec. 4.

2. Formalism

Throughout this work, we reanalyze *alpha* elastic scattering from ^{12}C, ^{16}O, ^{24}Mg, ^{28}Si, and ^{40}Ca at E_{Lab} = 130 MeV using different theoretical models. We recall that the *alpha*-nucleus interaction potential $U(R)$ may be written in the form:

$$U(R) = V(R) + iW(R) + V_C(R), \tag{1}$$

where $V(R)$ and $W(R)$ are the central real and imaginary nuclear parts of the optical potential, respectively and $V_C(R)$ is the repulsive coulomb potential, which is considered here due to a uniformly charged sphere of radius

$$R_C = r_C \left(A_P^{1/3} + A_T^{1/3}\right)$$

with $r_C = 1.3$ fm.

The imaginary part of the three used models is evaluated in the WS type

$$W(R) = W_o[1 + \exp\left(\left(R - R_I\right)/a_I\right)]^{-1},$$
$$R_I = r_I \left(A_P^{1/3} + A_T^{1/3}\right). \tag{2}$$

Here, W_o, r_I and a_I are the depth, radius, and diffuseness parameters of the imaginary potential, respectively. Merely, the real part is considered as one of the following forms.

2.1. Energy density function potential

The real *alpha*-nucleus potentials were calculated for the various investigated target nuclei in the context of EDF theory, for more details see Refs [35-37]. For a given density distribution $\rho(\mathrm{r})$, the energy of a system of fermions (*E*) is given by

$$E=\int \epsilon[\rho(\vec{r})]d\vec{r}, \tag{3}$$

where,

$$\begin{aligned}\epsilon[\rho(\vec{r})]=&\frac{3}{5}\left(\frac{\hbar^2}{2M}\right)\left(\frac{3\pi^2}{2}\right)^{\frac{2}{3}}\frac{1}{2}\left[(1-x)^{\frac{5}{3}}+(1+x)^{\frac{5}{3}}\right]\rho^{\frac{5}{3}}\\&+v(\rho,x)\rho+\frac{e}{2}\phi_c(\vec{r})\rho_p\\&-\frac{3}{4}\left(\frac{3}{\pi}\right)^{\frac{1}{3}}e^2\rho_p^{\frac{4}{3}}+\frac{\hbar^2}{8M}\eta(\nabla\rho)^2.\end{aligned} \tag{4}$$

Here x is the neutron excess, *M* is the mass of a nucleon and η is a free parameter adjusted to reproduce the nuclear masses. The average potential of a nucleon in the medium is $\nu(\rho,x)$ and is obtained from a Brueckner Hartree-Fock calculation using a realistic two-nucleon potential. The density dependence of $\nu(\rho,x)$ is given by,

$$\begin{aligned}\nu(\rho,x)=&\,b_1(1+a_1x^2)\rho\\&+b_2(1+a_2x^2)\rho^{\frac{4}{3}}+b_3(1+a_3x^2)\rho^{\frac{5}{3}}.\end{aligned} \tag{5}$$

The coulomb potential, ϕ_c, is related to the proton charge distribution , ρ_{P}, as follows

$$\phi_c(\vec{r})=e\int\frac{\rho_P(\vec{r}')}{|\vec{r}-\vec{r}'|}d\vec{r}' \tag{6}$$

The fourth term ($[3/4]\,[3/\pi]^{1/3}\,e^2\rho_p^{4/3}$) is the exchange correction to ϕ_c which can reproduce the observed nuclear masses at least as well as those obtained from any standard mass formula. The parameter x is zero for the examined projectile, targets and composite systems, respectively. Hence $\nu(\rho)$ reduces to

$$\nu(\rho)=b_1\rho+b_2\rho^{\frac{4}{3}}+b_3\rho^{\frac{5}{3}}, \tag{7}$$

where, $b_1=-741.28$, $b_2=1179.89$ and $b_3=-467.54$. The potential $V\,(R)$ between *alpha* and ^{12}C, ^{16}O, ^{24}Mg, ^{28}Si, and ^{40}Ca at a distance *R* is given by,

$$V(R)=E[\rho(\vec{r},R)]-E_\alpha[\rho_1(\vec{r},R)]-E_T[\rho_2(\vec{r},R)], \tag{8}$$

where ρ, ρ_1, and ρ_2 are, severally, density distribution functions of the composite system, *alpha* particle at *R* $=\infty$, and the target nuclei at *R* $=\infty$. In the sudden approximation [35]

$$\rho(\vec{r})=\rho_1(\vec{r})+\rho_2(\vec{r}). \tag{9}$$

For the projectile (*alpha* particle) density distribution $\rho_1\,(r)$, the Gaussian form is used as:

$$\rho_1(r)=4\left(\frac{\gamma}{\pi}\right)^{\frac{3}{2}}\exp(-\gamma r^2). \tag{10}$$

The root-mean-square radius (r.m.s) of the *alpha* particle using Eq. (10) at Eq. (4) with $\gamma = 0.45$ is 1.826 fm, and the binding energies are -20.049 MeV and -23.912 MeV when $\eta = 8$ and 6.2, respectively. These values are acceptably close to the observed values of -28.296 MeV and 1.7 fm [38].

For target nuclei density distribution $\rho_2\,(r)$, two choices of the density distributions are used; namely, matter (MT) and *alpha* cluster (CL) that used previously in different calculations [29,33,34] in the following form,

$$\rho(r)=\rho_0\left(1+\alpha r^2\right)\left[1+\exp\left(\frac{r-c}{a}\right)\right]^{-1}, \tag{11}$$

TABLE I. The matter (MT) and *alpha*-cluster (CL) density distribution of $4m$ nuclei in the form of two or three parameters Fermi function (2/3pF) $[29,33,34]$. In Eq.(4), the parameter $\eta=8,6.20$ for MT and CL densities, respectively.

Nucleus	Density type	ρ_0 fm^{-3}	ω fm^{-2}	c fm	a fm	r.m.s fm	B.E (MeV)[40]	Calc B.E (MeV)	Δ B.E (MeV)
^{12}C	MT	0.17533	0.00000	2.29400	0.43400	2.400	92.16	92.08	0.08
	CL	0.02319	0.23060	2.42075	0.23517	2.229	92.16	91.32	0.84
^{16}O	MT	0.16536	-0.05000	2.60800	0.51300	2.726	127.62	125.28	2.34
	CL	0.02483	0.23043	2.56391	0.24285	2.356	127.62	124.79	2.83
^{24}Mg	MT	0.16180	0.00000	2.98000	0.55100	3.086	198.26	194.17	4.09
	CL	0.02222	0.22619	2.93875	0.25057	2.662	198.26	193.47	4.79
^{28}Si	MT	0.16754	0.00000	3.14000	0.53700	3.146	236.54	234.54	2.00
	CL	0.02164	0.23379	3.05502	0.25914	2.773	232.54	227.16	5.38
^{40}Ca	MT	0.16985	0.16100	3.76600	0.58600	3.481	340.85	342.05	1.20
	CL	0.01878	0.21955	3.47117	0.29053	3.160	342.91	341.91	1.00

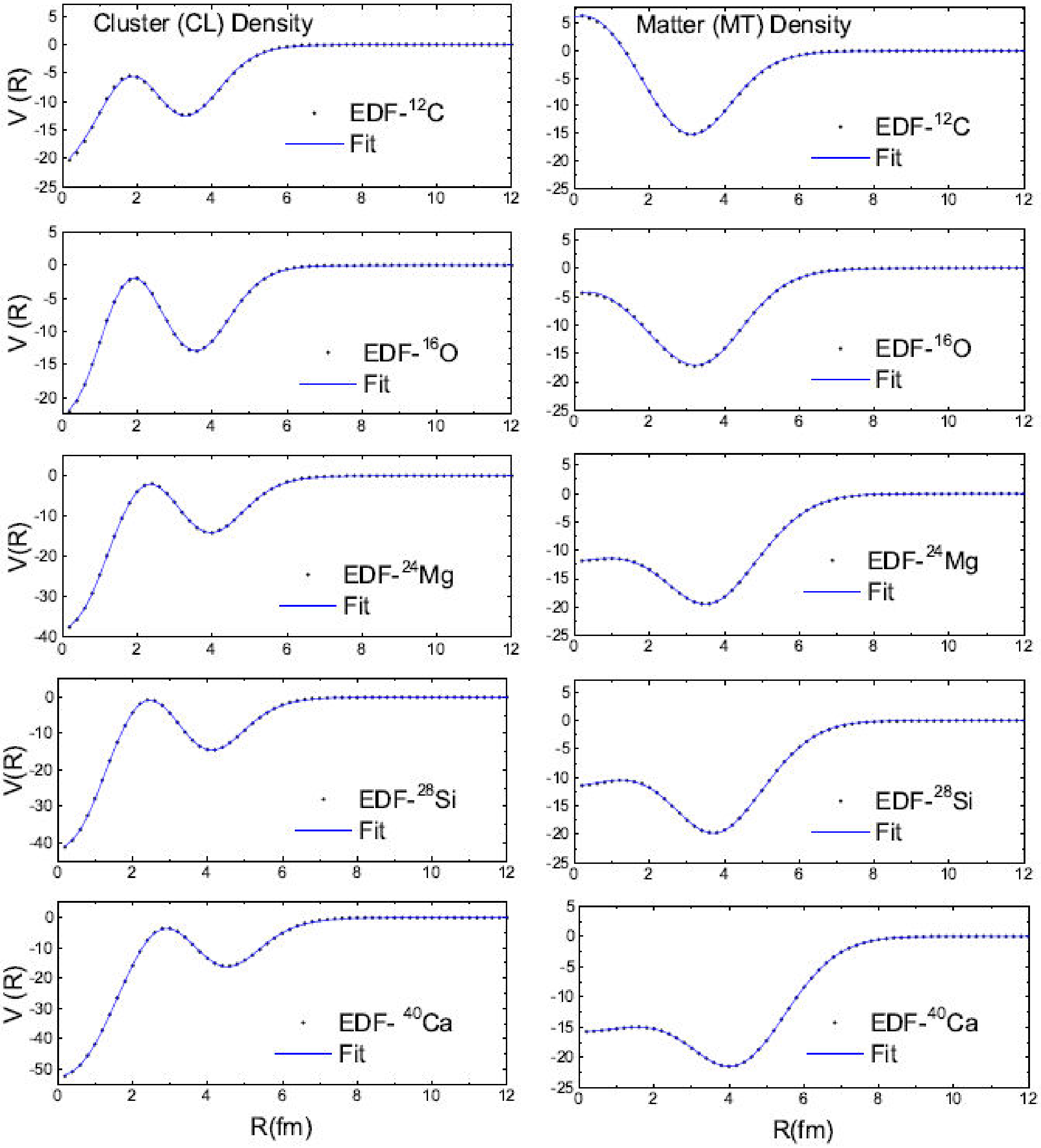

FIGURE 1. The generated energy density function (EDF) real potential based on *alpha*- cluster (CL) and matter (MT) density for various targets in comparison with the fitted potentials using Eq. (12).

where $\alpha = w$ for CL and $\alpha = w/c^2$ for MT densities with the Fermi parameters (2/3pF) listed in Table I.

The parameter η in Eq. (4) is chosen as 8 for MT and 6.2 for CL densities. Also, their corresponding root mean square radius and binding energies were calculated and written in Table I.

The results indicate clear agreement between the calculated and reference values of binding energies from [38]. Thus, by assigning $\eta = 8$ for MT densities and $\eta = 6.2$ for CL densities, the study ensures that the MT and *alpha*-CL density distributions accurately capture the underlying physics and characteristics of *4m* nuclei. These parameter choices are essential for obtaining meaningful results and facilitating a comprehensive understanding of the system under investigation. It is worth noting that the specific values of η chosen for MT and CL densities have been carefully determined and are supported by previous research and analysis [17-21,33]. Thus, this approach allows a consistency and comparability with existing literature and enables further exploration and investigation of the properties and behavior of *4m* nuclei.

The generated EDF potentials of Eq. (8), employing either MT or CL target densities for *4m* nuclei in the form of a two or three parameters Fermi function (2/3pF), are depicted in Fig. 1. These potentials were subsequently fitted to the equations

TABLE II. The fitted EDF potential parameters of Eq.(12) based on matter (MT) and *alpha*-cluster (CL) density distribution of $4m$ target nuclei in the form of parameters Fermi function.

Nucleus	Density	V_0 (MeV)	R$_0$ (fm)	a$_0$ (fm)	V$_1$ (MeV)	V$_2$ (MeV fm^{-1})	R$_1$ (fm)	D$_1$ (fm)	J_R^{Fit} (MeV fm^{-3})	J_R^{EDF} (MeV fm^{-3})
^{12}C	MT	-54.7411	3.8479	0.7226	61.7229	-3.0456	3.1222	0.4368	125.630	122.704
	CL	-17.4959	4.1244	0.5080	-6.8963	12.3919	1.3214	1.1252	98.4820	97.169
^{16}O	MT	-5.20010	3.7996	0.4943	5.0043	-6.0327	1.9486	2.6675	131.121	131.965
	CL	-19.5252	4.2998	0.5105	-7.4163	15.3889	1.3759	1.2524	83.5510	82.421
^{24}Mg	MT	-12.7844	4.0990	0.5853	10.4735	-5.9447	1.9797	3.1933	127.880	128.923
	CL	-28.5849	4.5097	0.5375	-19.6377	23.7195	1.6549	1.4066	76.4090	74.952
^{28}Si	MT	-12.5202	4.1844	0.5691	14.8904	-7.1299	1.9505	3.3171	119.350	120.382
	CL	-32.4433	4.6111	0.5445	-20.7542	25.5247	1.7141	1.5194	72.0950	70.603
^{40}Ca	MT	-16.1721	4.6626	0.7950	11.9757	-5.5798	1.9419	3.7937	117.265	117.112
	CL	-46.9107	4.9629	0.5708	-17.6938	24.3041	1.9021	1.9965	75.3317	73.479

$$V(R) = -V_0\left(1+\exp\left[\frac{(R-R_0)}{a_0}\right]\right)^{-1} + (V_1+V_2R)\exp\left[-\left(\frac{(R-D_1)}{R_1}\right)^2\right], \qquad (12)$$

with the corresponding parameters provided in Table II. Noting that for first time the term (V_2R) is added in Eq. (12) which is different than the used NM EDF-derived by Basak *et al.* "for example, see Ref. [21]".

To assess the accuracy of the fit, the real volume integral (J_R) for both the EDF-derived potential and the potentials obtained from the fitted equation for each system are calculated according to the following relation

$$J_R = \frac{4\pi}{A_P A_T}\int_0^\infty V(r) r^2\, dr. \qquad (13)$$

and indicated in the last two columns of Table II. The results show a consistency between the obtained values. Furthermore, it is obvious from Fig. 1, that for both type of fitted potentials using Eq. (12) are in excellent agreement with the present EDF calculations of Eq. (8), the potentials depth increases with increasing the target mass number, and MT potentials are shallower than CL potentials. Also, it is noted from this figure that ^{12}C has a repulsive central MT-potential which differs than the attractive central MT-potential of other targets. So, the corresponding resulting cross sections may be affected by this different behavior. This will be clarified later on. However, it is expected that both potentials can still accurately describe the calculated cross-section, although they are qualitatively different according to variations in their functional form, strength and range. This is supported by the close values of the calculated binding energies (see Table I) and the real volume integral (J_R) values for EDF, MT, and CL-fitted potentials (see Table II).

The resultant real potentials of Table II are multiplied by a real renormalization factor, N_R. This factor is considered as adjustable parameters, and it is allowed to be varied freely in addition to three WS imaginary potential parameters [see Eq. (2)] until the theoretical calculations of scattering cross section achieve the best possible agreement with the experimental data. These four parameters, namely, N_R and three WS imaginary potential parameters of Eq. (2) are given in Table III and denoted as EDF-1 for either MT or CL target densities used.

2.2. Single folding cluster (SFC) potential

We apply the *alpha*-single folding cluster model for the ^{12}C, ^{16}O, ^{24}Mg, ^{28}Si, and ^{40}Ca nuclei. Considering this objective, the density distributions of the target nuclei are obtained over the *alpha*-CL density distribution and *alpha-alpha* effective interaction using BiFold code [39] and DFPOT code [40], which is expressed by:

$$V(R) = \int \rho_2(\mathbf{r}_2)\nu_{\alpha-\alpha}(|\mathbf{s}|)\, d\mathbf{r}_2, \quad \mathbf{s} = \mathbf{R} - \mathbf{r}_2. \qquad (14)$$

For the *alpha*-CL densities, $\rho_2(r_2)$, we used a two or three parameter Fermi density (2/3pF) of Eq. (11) that used in the previous section and indicated in Table I. The interaction potential $\nu_{\alpha-\alpha}$ is taken in the Buck form [41] as

$$\nu_{\alpha-\alpha}(r) = -122.6\exp(-0.22r^2). \qquad (15)$$

Comparing the real WS potentials, Fig. 2 illustrates the non-renormalized (N_R=1) real SFC potentials. As EDF potentials, the resultant real potential is multiplied by N_R and denoted as SFC potential in our study. So, the best agreement of calculated scattering cross section with experimental data is attained using four free parameters, namely, N_R and three WS imaginary potential parameters of Eq. (2). The acquired parameters included in Table III.

TABLE III. The Optical potential parameters obtained from the best fit to the experimental data for *alpha*- particles scattered from the considered targets within different models based on Woods-Saxon (WS), single folding cluster (SFC), energy density functional for cluster (EDF-CL) and matter density (EDF-MT) potentials.

Density Type	Potentials	N_R	Vo/M (MeV)	r$_o$ /R1 (fm)	a_o /R2 (fm)	W$_o$ (fm)	r_I (fm)	a_I (fm)	J_R (MeV. fm^3)	J_I (MeV. fm^3)	χ^2	σ_R (mb)
alpha + ^{12}C												
	WS	—–	104.43	0.725	0.788	15.68	1.121	0.489	359.9	126.3	1.36	808.8
CL	SFC	0.76	—–	—–	—–	20.29	0.951	0.724	314.50	120.90	2.10	836.0
CL	EDF-1	2.08	—–	—–	—–	22.93	1.020	0.620	206.06	153.74	25.93	862.8
	EDF-2	1.0	1.186	2.01	23.04	22.93	1.020	0.620	210.1	153.74	25.93	862.8
MT	EDF-1	1.79	—–	—–	—–	20.29	1.020	0.620	219.59	136.09	17.89	840.8
	EDF-2	1.0	0.8	3.04	18.89	20.29	1.020	0.620	224.2	136.09	17.89	840.8
alpha + ^{16}O												
	WS	—–	92.27	0.848	0.740	15.47	1.790	0.441	396.10	92.30	1.71	943.3
CL	SFC	0.64	—–	—–	—–	14.53	1.01	0.895	263.10	104.2	3.85	1023
CL	EDF-1	2.18	—–	—–	—–	179.54	0.389	0.899	182.49	206.71	18.71	1005
	EDF-2	1.0	1.19	1.65	21.8	179.54	0.389	0.899	176.9	206.71	18.71	1005
MT	EDF-1	2.07	—–	—–	—–	30.94	1.12	0.42	278.49	213.36	19.12	981.8
	EDF-2	1.0	1.08	2.23	15.18	30.94	1.12	0.42	264.1	213.36	19.12	981.8
alpha + ^{24}Mg												
	WS	—–	87.15	0.950	0.728	20.12	1.171	0.555	375.6	139.90	1.57	1248
CL	SFC	1.17	—–	—–	—–	24.70	0.975	0.855	437.1	123.40	2.48	1307
CL	EDF-1	1.94	—–	—–	—–	54.46	0.735	0.915	148.12	143.73	16.27	1218
	EDF-2	1.0	0.96	2.91	21.84	54.46	0.735	0.915	146.64	143.73	16.27	1218
MT	EDF-1	1.65	—–	—–	—–	31.62	1.15	0.40	211.38	198.87	11.83	1143
	EDF-2	1.0	0.66	3.31	18.64	31.62	1.15	0.40	180.88	198.87	11.83	1143
alpha+^{28}Si												
	WS	—–	88.59	0.900	0.723	20.89	1.120	0.527	317.8	172.0	1.41	1188
CL	SFC	1.77	—–	—–	—–	25.52	1.960	0.622	445.90	233.20	5.42	1472
CL	EDF-1	2.27	—–	—–	—–	48.07	0.751	0.929	163.61	128.88	9.87	1290
	EDF-2	1.0	1.3	2.57	24.25	48.07	0.751	0.929	160.35	128.88	9.87	1290
MT	EDF-1	1.89	—–	—–	—–	35.33	1.12	0.42	225.33	195.43	11.19	1207
	EDF-2	1.0	0.9	2.91	19.46	35.33	1.12	0.42	184.5	195.43	11.19	1207
alpha+ ^{40}Ca												
	WS	—–	102.24	0.898	0.778	19.16	1.158	1.153	315.40	107.30	1.29	1439
CL	SFC	1.07	—–	—–	—–	25.52	1.096	0.622	445.9	124.6	5.42	1472
CL	EDF-1	2.16	—–	—–	—–	36.91	0.809	1.113	162.68	112.31	10.62	1694
	EDF-2	1.0	1.23	2.56	17.26	36.91	0.809	1.113	155.60	112.31	10.62	1694
MT	EDF-1	1.84	—–	—–	—–	42.54	1.12	0.45	216.39	208.93	10.27	1433
	EDF-2	1.0	0.87	1.28	23.6	42.54	1.12	0.45	145.6	208.93	10.27	1433

2.3. Phenomenological woods-saxon (WS) potential

In order to provide a more comprehensive analysis of the elastic scattering results, the phenomenological WS potential is evaluated in this study. In this context, the real part of the optical model potential is assumed as WS type, which is expressed as

$$V(R) = V_o[1 + \exp\left(\left(R - R_o\right)/a_o\right)]^{-1}, R_o = r_o\left(A_P^{1/3} + A_T^{1/3}\right), \tag{16}$$

where $V_o,\ r_o$ and a_o are the depth, radius and diffuseness parameters for real potentials, respectively.

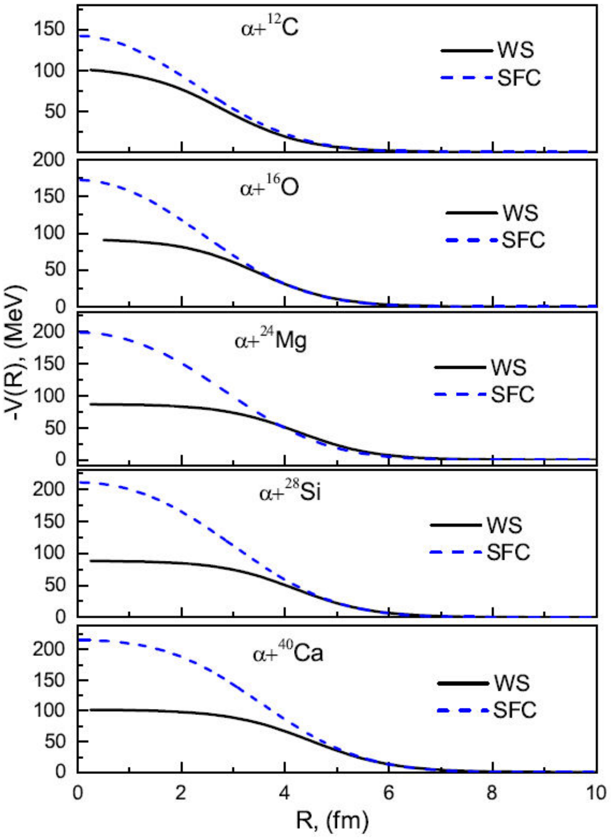

FIGURE 2. Comparison between real part of phenomenological Woods-Saxon (WS) potential and that of non renormalized single folding cluster(SFC) potential for different targets.

Accordingly, the best agreement of calculated scattering cross section with experimental data is accomplished by varying six parameters for total nuclear interaction potential (real and imaginary parts). The obtained parameters reported in Table III.

It is detected from this figure that the depth of the calculated potentials increases with increasing the target mass number. On the other hand, WS potentials show a shallower depth than SFC potentials by nearly a factor two. Thus, this leads to the necessity to normalize the employed SFC potentials for successful prediction of scattering cross section data. Also, it is shown that the calculated potentials behave in the surface in a manner that depends on the target nucleus. Meaning that, the similarity in potentials is found within radial distances greater than 3, 3.5, 4 and 4.5 fm for ^{12}C, ^{16}O, ^{24}Mg, ^{28}Si, and ^{40}Ca, respectively. As a consequence, these potential differences will have impacts on the corresponding resulting cross sections.

3. Results and discussions

3.1. Elastic scattering analysis within energy density functional (EDF) potential

The generated *alpha* +^{12}C, ^{16}O, ^{24}Mg, ^{28}Si, and ^{40}Ca EDF real potentials using target densities as either CL or MT form in addition to their fitted EDF potentials at 130 MeV are shown in Fig. 1. The (EDF-1)-MT and (EDF-1)-CL fitted potentials, along with the imaginary WS potentials, were entered into the FRESCO code [42]. In order to identify the optimal potential parameters, the calculations were refined using the (χ^2) minimization SFRESCO search code [42]. The resulting parameters were recorded in Table III.

The calculated elastic scattering cross sections in Fig. 3 (right panel) yielded similar behavior and satisfactory reproduction of the experimental data at 130 MeV [22]. As shown, there are significant differences between calculated and experimental data at the mid angles (mainly in the magnitude of the interior repulsive potential region) in some cases. This is more clear in case of ^{12}C target while using the CL potential represents a slightly more under estimation of data at the mid angles than MT-potential. This means that Gaussian function Eq. (10) used in describing *alpha* density doesn't determine the magnitude of its central part very well and hence, the repulsive interior part of the potential is not well described by the EDF calculations. Also, it is noticeable that using the shallowest MT density reproduces the data with lower N_R values than using CL density.

For solving the increase problem of the real renormalization factor N_R than unity, we have been used the non-renormalized fitted real potentials with (N_R =1) plus a repulsive real potential ΔV as EDF-2 potentials. ΔV is put-upon as a correction of the form

$$\Delta V\,(R) = F\,(R)\,V(R), \tag{17}$$

where $V(R)$ is the fitted EDF potentials obtained from Eq. (12), and $F(R)$ is expressed in the Gaussian form as follows:

$$F\,(R) = M\exp\left[-\alpha\left(\frac{R-R_1}{R_2}\right)^2\right]. \tag{18}$$

The used additive potential $\Delta V(R)$ is characterized by three parameters (the amplitude factor M, the radius R_1 at which F(R) is maximum M, and the full-width half maximum radius R_2). The parameter α is set as 2.7573 [43].

One again, the optimal parameters in addition with the same imaginary parameters in renormalized EDF potentials (EDF-1) are listed in Table III.

3.2. Elastic scattering analysis within SFC and WS potentials

The generated *alpha* +^{12}C, ^{16}O, ^{24}Mg, ^{28}Si, and ^{40}Ca SFC real potentials using BiFold code [39] and DFPOT code [40], as well as phenomenological WS real potentials at 130 MeV are shown in Fig. 2. The produced potentials are used to calculate the elastic scattering differential cross sections of the investigated systems using Fresco code [42]. The resulting best fitting parameters of these calculations are listed in Table III. The comparisons between the experimental data and theoretical calculations are displayed in Fig. 3 (left panel).

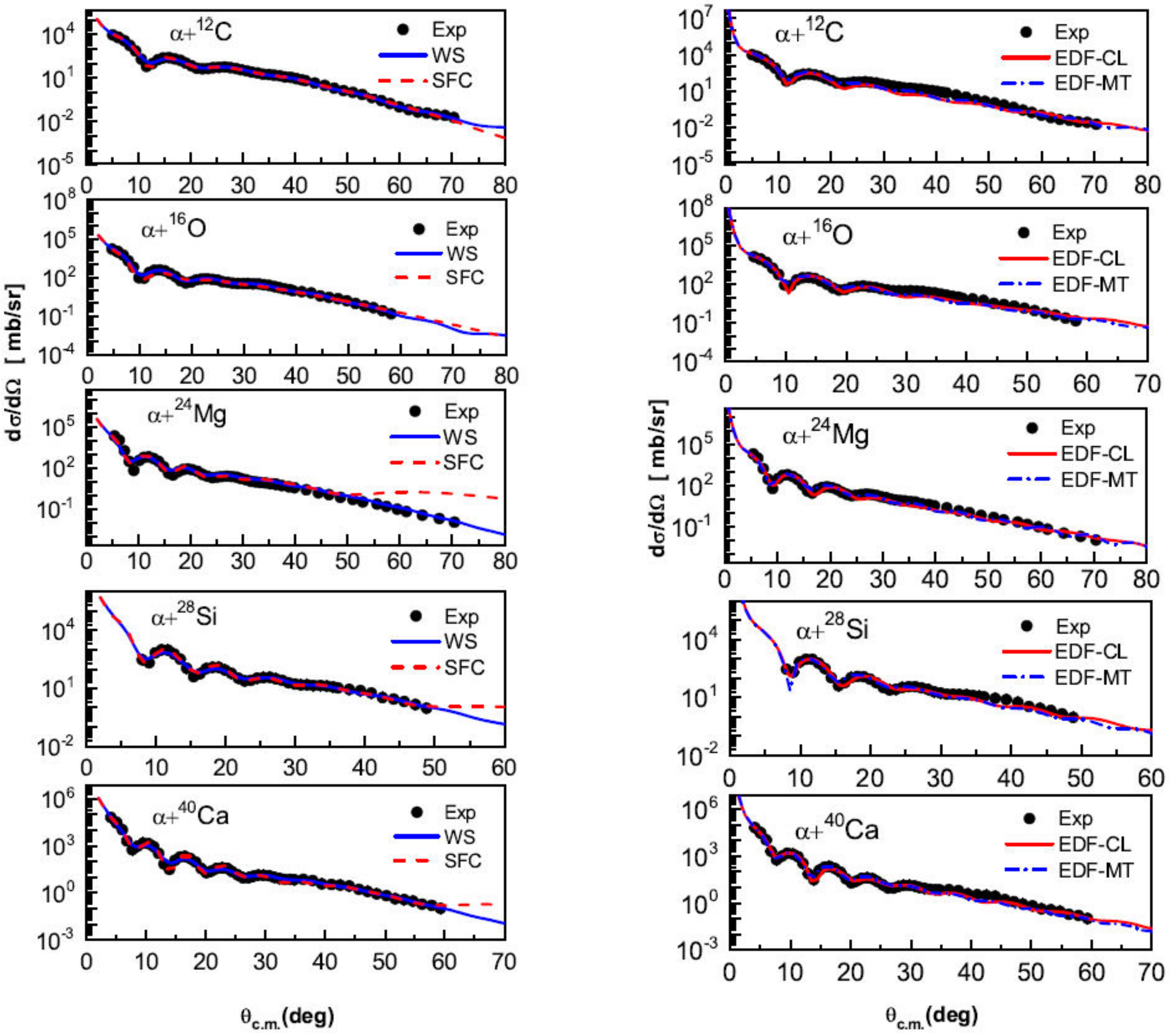

FIGURE 3. Experimental angular distribution from Ref [22] and fits for *alpha*-particles elastic scattering at $E_{lab} = 130$ MeV from five target nuclei using different models based on ; a) phenomenological Woods-Saxon (WS) potential and single folding cluster (SFC) potential in right panel and b) EDF potential with matter (MT) and cluster (CL) densities in left panel.

It is evident, in general, that the SFC model is successful in predicting the experimental differential cross sections all over the measured angular range for all targets, except for ^{12}C nucleus. The rainbow scattering is well reproduced by the SFC potentials. In this SFC model, we have only four searching parameters, namely the repulsive depth of the *alpha-alpha* effective interaction and the three parameters of the WS imaginary potentials. However, it was essential to renormalize the real SFC potentials by the factors from 0.64 to 1.77 in order to successfully reproduce the scattering data as indicated in Table III. This success is comparable to those produced using analysis based on phenomenological WS potentials with free searching on six parameters. It is noticeable that the agreement between theoretical calculations and experimental data is almost perfect for the WS potentials at small and large angles.

We have also calculated both volume integral (J_R), real and imaginary (J_I), as well as χ^2 values accompanied by different investigated potentials. Similarly as the J_R of Eq. (13), the J_I is calculated according to the following relation,

$$J_I = \frac{4\pi}{A_P A_T} \int_0^\infty W(r)\ r^2 dr. \tag{19}$$

Figure 4 represents the change of J_R and J_I quantities with target mass at incident energy 130 MeV that play an important role in demonstrating the strength of the evaluated potentials. The different behavior of $J_{R,I}$ for each model results from the values of their related potential depths used in the calculations as listed in Table III. Precisely, it will be illustrated in the succeeding sentences.

It is demonstrable from this figure panel (a), that the dependence of the target mass on the extracted J_R and J_I values shows a remarkable increase for ^{16}O except for J_R attached to EDF-CL. This is attributed to the smallest value of the full-width half maximum radius R_2 (1.65) as seen in Table III. Then again, two observations about the variation of the J_I values from panel (b) of the same figure are illustrated as: (1) it is similar for SFC and WS potentials but the situation is

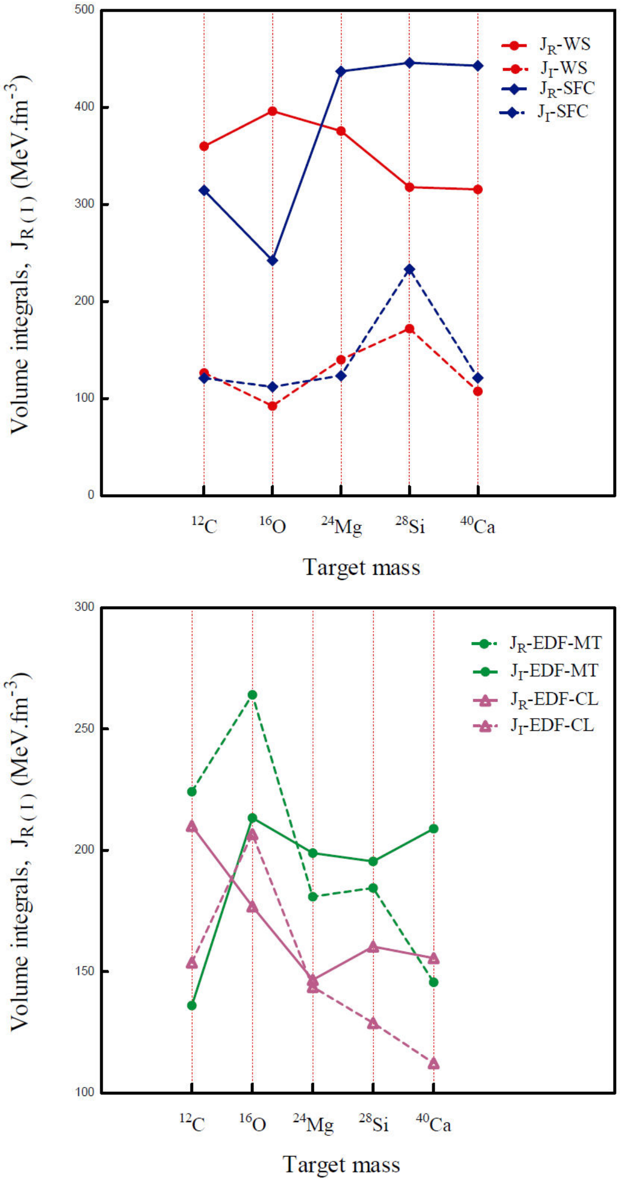

FIGURE 4. a) Variation of real (J_R) and imaginary (J_I) volume integral with target mass using EDF potentials with matter (MT) and cluster (CL) densities in panel and, b) Woods-Saxon (WS) and single folding cluster (SFC) potentials in panel.

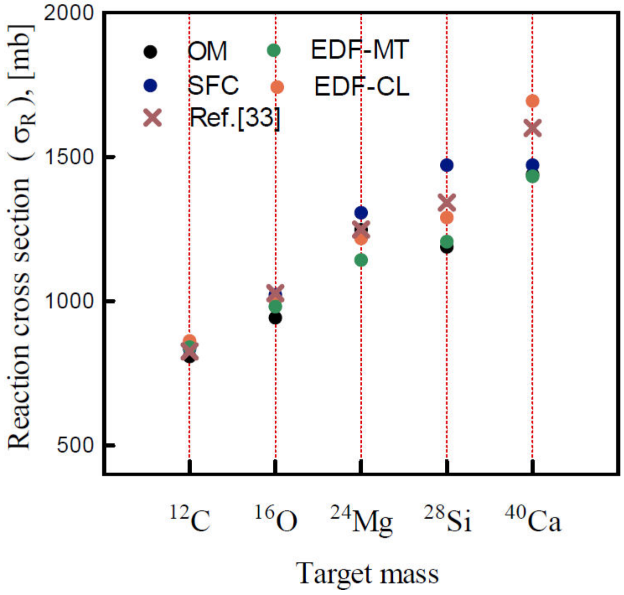

FIGURE 5. Variation of reaction cross section (σ_R) with target mass using EDF potentials with matter (MT) and cluster (CL) densities, Woods-Saxon (WS) and single folding cluster (SFC) potentials.

different for J_R values, and (2) it slightly increases with the increase of target mass up to $A = 28$ of silicon in contrast to EDF potentials. This behavior may be attributed to the more expected inelastic channels to be opened at this energy for this target. It is confirmed by relatively high real normalization factor (N_R = 1.77) in case of *alpha* + ^{28}Si reaction. It is worth noting that using CL density within EDF-1 potentials provides also the highest real normalization factor (N_R = 2.27) for the same reaction.

The agreement between the theoretical calculations and experimental data for each system is examined by minimizing the value χ^2. It is weighted with experimental uncertainties to account for measurement errors and defined by the following expression

$$\chi^2 = \frac{1}{N}\sum_{i=1}^{N}\left(\frac{\sigma(\theta_i)^{\text{cal}} - \sigma(\theta_i)^{\text{exp}}}{\Delta\sigma(\theta_i)}\right)^2. \qquad (20)$$

Here, N is the number of data points, and are the calculated and experimental differential cross sections and is the relative uncertainty in experimental data. In Table III, the smallest values ($\sim 1.3 - 1.7$) and ($\sim 2 - 5.5$) are observed for the WS and SFC results, respectively. A lower value of provides a better description of the experimental data in terms of the selected theoretical representation. Then again, the highest values ($\sim 11 - 26$) are observed for EDF potentials. As listed in Table III, EDF potentials has a close values for each target except for ^{12}C. While using the CL-EDF potentials, a remarkable higher values (∼26) is shown for ^{12}C than MT-EDF potentials (∼28) according to the above discussed reasons.

Likewise, the reaction cross section (σ_R) is a fundamental quantity that characterizes the probability of a specific reaction occurring during nuclear interactions. It depends on factors such as the energy of the particles involved, the nature of the interaction, and the properties of the target material. Experimental techniques, involving collision experiments and detection of reaction products, are used to measure reaction cross-sections, while theoretical models provide predictions when direct measurements are challenging. Hence, the calculated σ_R values using the above described four models are presented in Table III for each reaction. Our calculated σ_R values are compared with those obtained by previous SFC analyses [33] and are displayed in Fig. 5. As it is clear, the σ_R values increase linearly as target mass increase. Additionally, the obtained values using EDF-CL potentials are in agreement with those predicted by SFC potential using *alpha*-CL density based on EDF optimization procedure [33] for *alpha* + ^{12}C, ^{16}O and ^{24}Mg, and close to that obtained for *alpha* + ^{28}Si and ^{40}Ca. This comparison verifies the success of the present EDF-CL potentials especially for light targets. Thus, it can be concluded that the similar reaction cross sections for different models can indicate similar results for experimental data.

3.3. Inelastic scattering potential

In the present study, in order to test further the nuclear potential parameters, coupled channels (CC) calculations for the inelastic scattering to the different low lying excited states of the chosen targets ^{12}C, ^{16}O, ^{24}Mg, ^{28}Si, and ^{40}Ca are carried out within FRESCO code [44]. The same potential parameters which were used in fitting the elastic scattering data were utilized to reproduce the inelastic scattering cross sections. The nuclear part of the potential is deformed using the deformation length δ given by $\delta_\lambda = \beta_\lambda . R$, while the nuclear and Coulomb matrix elements in the rotational model are related by:

$$M_n(E\lambda) = \frac{3Z\beta_\lambda R^\lambda}{4\pi}. \tag{21}$$

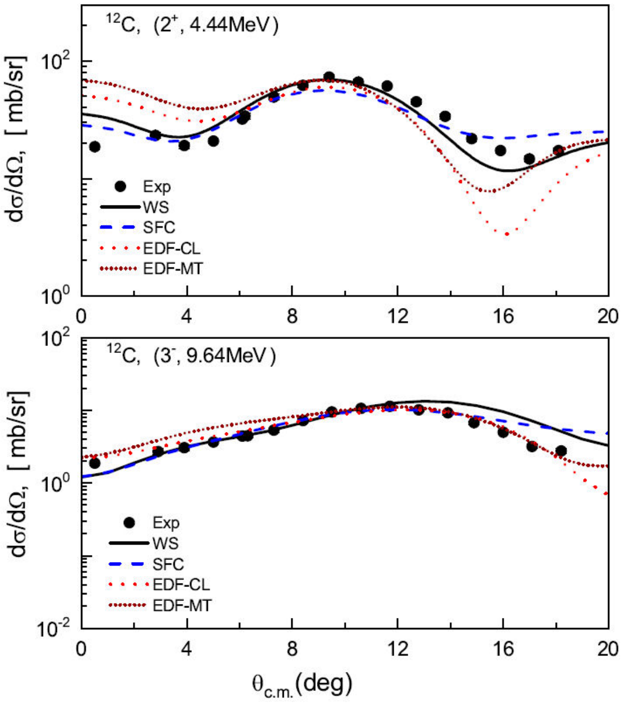

FIGURE 6. Inelastic scattering cross sections for different excited states as indicated in figure for *alpha*-^{12}C obtained with the CC calculations based on different potentials; Woods-Saxon (WS), single folding cluster (SFC), energy density functional for cluster (EDF-CL) and matter density (EDF-MT) potentials in comparison with experimental data at 130 MeV. The experimental data is taken from Ref. [22].

Here β is the deformation parameter, and λ is the multipolarity. The transitions to these states are calculated using the form factors:

$$V_\lambda(r) = -\frac{\delta_\lambda}{\sqrt{4\pi}} \frac{dU_N(r)}{dr}. \tag{22}$$

Reduced transition probability $Mn(E\lambda)$is related to the electric quadruple transition probability $M(E\lambda)$by the relation

$$Mn(E\lambda) = \frac{M(E\lambda)}{\left[(-1)^{[I-I'+|I-I'|/2}\sqrt{2\text{I}+1}\,\langle IK\lambda 0\,|I'K\,\rangle\ \right]}, \tag{23}$$

where $\langle IK\lambda 0\,|I'K\,\rangle$ is the Clebsh-Gordan coefficient.

In the CC calculations the deformation length δ was taken as a free parameter which reasonably reproduced the inelastic cross section for the different transitions studied: *alpha* + ^{12}C system with transition to the (2_1^+, E_x = 4.44 MeV) and (3_1^- , E_x = 9.64 MeV) ^{12}C excited states, *alpha* + ^{16}O system with transition to the (2_1^+, E_x = 9.84 MeV), (3_1^-, E_x = 6.13 MeV), (4_1^+, E_x = 10.36 MeV) ^{16}O excited states,

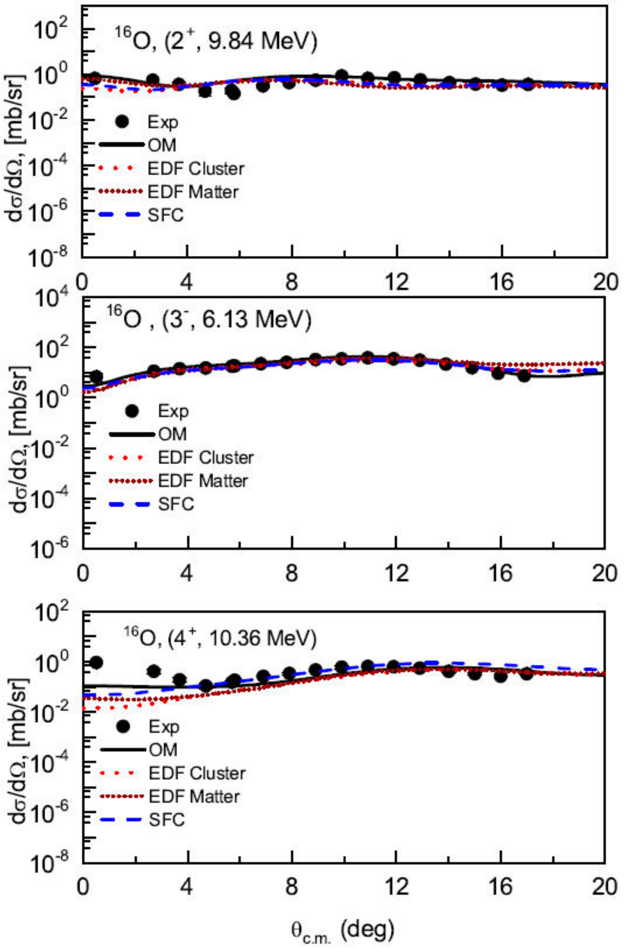

FIGURE 7. Same as Fig. 6 but for ^{16}O. The experimental data is taken from Ref. [22].

TABLE IV. The extracted deformation length (δ) parameter in fm for different excited low lying states of investigated targets within CC method based on Woods-Saxon (WS), single folding cluster (SFC), energy density functional for cluster (EDF-CL) and matter density (EDF-MT) potentials.

Target	Potential	Excited state (J^{π})	Excitation energy (E_x)	Deformation Length (δ)	Previous work
^{12}C	WS	2^+	4.44	1.239	1.27[45]
	SFC			1.214	1.07±0.05[46]
	EDF-CL			1.214	1.08[47]
	EDF-MT				
	WS	3^-	9.64	1.321	0.68[45]
	SFC			1.239	0.67[47]
	EDF-CL			0.751	
	EDF-MT			0.751	
^{16}O	WS	2^+	9.84	0.14	0.1[38]
	SFC			0.14	
	EDF-CL			0.14	
	EDF-MT			0.14	
	WS	3^-	6.13	1.1	1.41 [48]
	SFC			1.21	
	EDF-CL			1.1	
	EDF-MT			1.1	
	WS	4^+	10.36	0.20	0.49[38]
	SFC			0.28	
	EDF-CL			0.20	
	EDF-MT			0.20	
^{24}Mg	WS	2^+	1.37	1.24	1.63 [49]
	SFC			1.07	1.50 ± 0.15 [50]
	EDF-CL			1.366	
	EDF-MT			1.366	
	WS	4^-	6.01	1.529	0.48 [49]
	SFC			1.129	
	EDF-CL			0.761	
	EDF-MT			0.761	
^{28}Si	WS	2^+	1.78	1.366	1.25 [49]
	SFC			1.07	1.22 ± 0.14 [50]
	EDF-CL			1.24	
	EDF-MT			1.24	
	WS	4^-	4.62	1.633	0.32 [50]
	SFC			1.632	
	EDF-CL			0.53	
	EDF-MT			0.53	
^{40}Ca	WS	2^+	3.9	0.42	0.37[49]
	SFC			0.43	0.37 ± 0.07 [50]
	EDF-CL			0.43	
	EDF-MT			0.43	
	WS	3^-	3.74	1.1	0.90 [49]
	SFC			1.1	
	EDF-CL			1.1	
	EDF-MT			1.1	

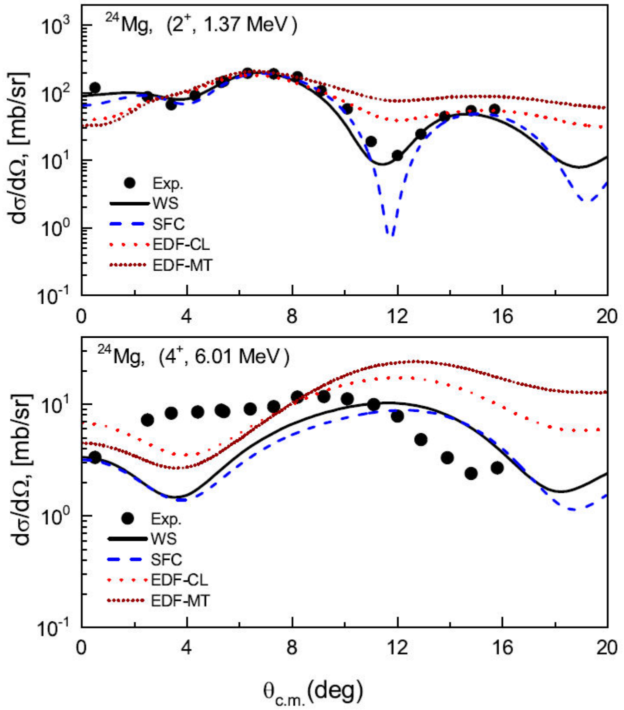

FIGURE 8. Same as Fig. 6 but for ^{24}Mg. The experimental data is taken from Ref. [22].

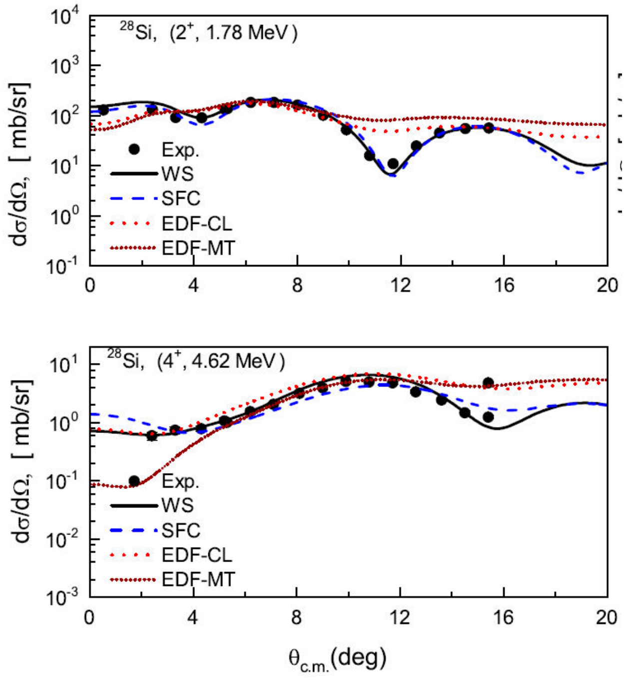

FIGURE 9. Same as Fig. 6 but for ^{28}Si. The experimental data is taken from Ref. [22].

alpha + ^{24}Mg system with transition to the (2_1^+, E_x = 1.37 MeV) and (4_1^+, E_x = 6.01 MeV) ^{24}Mg excited states, *alpha* + ^{28}Si system with transition to the (2_1^+, E_x = 1.78 MeV) and (4_1^+, E_x = 4.62 MeV) ^{28}Si excited states, and *alpha* + ^{40}Ca system with transition to the (2_1^+, E_x = 3.9 MeV) and (3_1^-, E_x = 3.74 MeV), ^{40}Ca excited states. The optimal extracted quadrupole (δ_2), octupole (δ_3), and hexadecapole (δ_4) deformation lengths for the excited states of the studied targets are listed in Table IV, and compared to other previous values from literature [45-50].

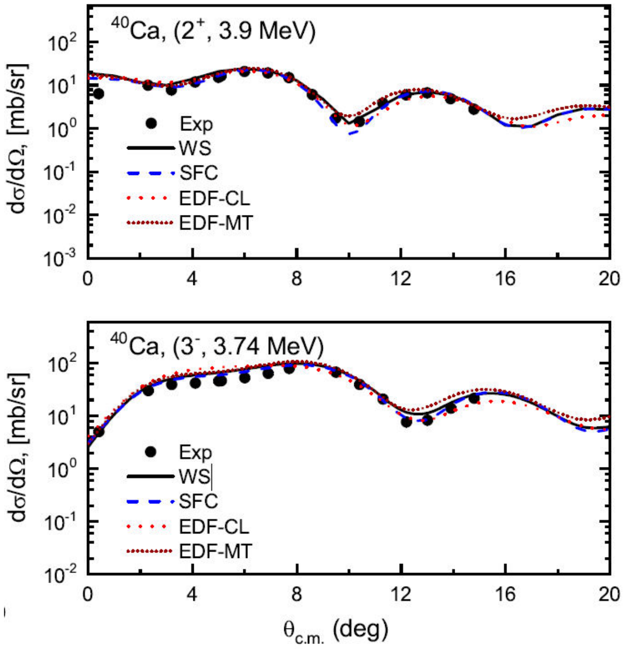

FIGURE 10. Same as Fig. 6 but for ^{40}Ca. The experimental data is taken from Ref. [22].

The comparison between the experimental inelastic angular distributions and CC calculations are shown in Figs. 6-10 for the low lying excited states (2_1^+, 3_1^-, and 4_1^+) of the considered targets.

It was found that the calculated scattering cross sections with the EDF-MT potentials are systematically smaller than those with EDF-CL potentials with similar behavior for most of states as presented in Figs. 6-10 and those with both potentials overestimate the cross sections at $\theta < 8°$ for the 3_1^- state in ^{12}C as elucidated in Fig. 6. Also, both calculations fail in reproducing the state 4_1^+experimental data of ^{24}Mg and success in description of the experimental data related to different states of ^{16}O and ^{40}Ca. In Fig. 9, the angular distributions of the experimental data for the 4_1^+, ^{28}Si state is slightly shifted to forward angles compared with the EDF- calculations and underestimate of data at $\theta < 5°$ connected to EDF-MT potentials.

Furthermore, from the same figures, we conclude that the current SFC and WS calculations reproduces reasonably well the experimental data except for the 4_1^+ ^{24}Mg state as well as EDF-potentials. Additionally, it was found that the calculated scattering cross sections within the SFC potentials are consistently smaller than those with WS potentials over the whole angular range for the 4_1^+ state as presented in Fig. 8 and those with both potentials overestimate the cross sections at $\theta > 12°$ for the 3_1^- state in ^{12}C as clarified in Fig. 6. For the 4_1^+ ^{28}Si state (see Fig. 9), the angular distributions of the experimental data is slightly shifted to forward angles compared with the SFC calculations. One can see that the SFC and WS calculations successfully reproduce the 2_1^+ state cross sections with good description of amplitude and diffraction pattern in all target nuclei which is presented in Figs. 6-10. Similar conclusion is reported in Refs. [51,52] for ^{28}Si and ^{16}O, respectively.

4. Conclusion

In the current study, we applied EDF- generated potentials for CL and MT densities with new fitted parameters for the first time to analyses the elastic and inelastic scattering cross sections of α + ^{12}C, ^{16}O, ^{24}Mg, ^{28}Si, and ^{40}Ca reactions at 130 MeV. To judge the performance of the EDF potentials, the work also presents the results of analyses on the cross section scattering data in terms of the phenomenological WS and the SFC potentials based on the optical model in addition to the EDF ones.

The analysis showed that all the four potentials provide a satisfactory description of the general trends and magnitudes of the experimental data. In order to reproduce the data accurately, the strength of the real potential needed to be normalized by factor N_R in range between $(0.64-1.77)$ according to the SFC potentials and $(1.65-2.27)$ according to the EDF-1 potentials. So, a correction is added and a new parameter are obtained for the latter for first time without normalization.

As to be anticipated, the inelastic calculations for the low lying excited states (2_1^+, 3_1^-, and 4_1^+) using four potentials agree best with experimental data for those nuclei not being deformed; ^{16}O and ^{40}Ca. With the fixed low lying excited state (2_1^+), some information on the nuclear deformation length may be already gained from the present optical model analysis: there is a pronounced correlation between the volume integrals of the imaginary part of both, WS and SFC potentials and the nuclear deformation length $\delta_.$

Acknowledgement

The authors are thankful to the Deanship of Graduate Studies and Scientific Research at University of Bisha for supporting this work through the Fast-Track Research Support Program. The authors extend their appreciation to the Research Center for Advanced Materials Science (RCAMS), King Khalid University, Saudi Arabia, for funding this work under grant number KKU/RCAMS/0022/23.

Declaration of Competing Interest

The authors declare that they have no known competing financial interests or personal relationships that could have appeared to influence the work reported in this paper.

---

1. M. Freer, *The Euroschool on Exotic Beams, Vol. IV, Lecture Notes in Physics* 879, (Springer Verlag, Berlin, Heidelberg, 2014), `https://10.1007/978-3-642-45141-6`.
2. J.A. Wheeler, *On the Mathematical Description of Light Nuclei by the Method of Resonating Group Structure*, Phys. Rev. **52** (1937) 1107, `https://doi.org/10.1103/PhysRev.52.1107`.
3. D.M. Brink, *The alpha-particle model of light nuclei*, Proceedings of the International School of Physics ,Enrico Fermi, Course XXXVI, edited by C. L. Bloch (Aca-demic press, New York, 1966) 247.
4. B. Zhou *et al.*, *Nonlocalized cluster dynamics and nuclear molecular structure*, Phys. Rev. C **89** (2014) 34319, `https://doi.org/10.1103/PhysRevC.89.034319`.
5. B. Buck, A.C. Merchant, S.M. Perez,*Systematics of alpha-cluster states above double shell closures*, Phys. Rev. C **51** (1995) 559, `https://doi.org/10.1103/PhysRevC.51.559`.
6. A. Tohsaki, H. Horiuchi, P. Schuck, G. Roepke,Colloquium:*Status of α-particle condensate structure of the Hoyle state*, Rev. Mod. Phys. **89** (2017) 11002, `https://doi.org/10.1103/RevModPhys.89.011002`.
7. H. Horiuchi, K. Ikeda,*A Molecule-like Structure in Atomic Nuclei of $^{16}O*$ and ^{10}Ne*, Prog. Theor. Phys. **40** (1968) 277, `https://doi.org/10.1143/PTP.41.1386`.
8. M. Freer, A.C. Merchant,*Developments in the study of nuclear clustering in light even-even nuclei*, J. Phys. G: Nucl. Part. Phys. **23** (1997) 261, `https://doi.org/10.1088/0954-3899/23/3/002`.
9. N. Zoghi-Foumani, M.R. Shojaei, A.A. Rajabi,*A new non-microscopic study of cluster structures in light alpha-conjugate nuclei*, Chin. Phys. C **41** (2017) 14104, `https://dx.doi.org/10.1088/1674-1137/41/1/014104`.
10. F. Michel, *α-clustering in the ground state of ^{40}Ca*, Phys. Lett. B **60** (1976) 229, `https://doi.org/10.1016/0370-2693(76)90287-2`.
11. Th. Delbar *et al.*, *Elastic and inelastic scattering of alpha particles from $^{40,44}Ca$ over a broad range of energies and angles*, Phys. Rev. C **18** (1978) 1237, `https://doi.org/10.1103/Phys.Rev.C.18.1237`.
12. D. T. Khoa,*Exchange effects in nuclear rainbow scattering*, Nucl. Phys. A **484** (1988) 376, `https://doi.org/10.1016/0375-9474(88)90077-2`.
13. M. EL-Azab Farid, Z. M. M. Mahmoud and G.S.Hassan,*α-clustering folding model*, Phys.Rev.C 64 (2001)014310, `https://doi.org/10.1103/PhysRevC.64.014310`.
14. M. Karakoc and I. Boztosun, *α-α double folding cluster potential description of the ^{12}C+^{24}Mg system*, Phys. Rev. C **73** (2006) 047601, `https://doi.org/10.1103/PhysRevC.73.047601`.

15. M. N. A. Abdullah *et al.*,*Cluster structure of* ^{40,44,48}*Ca*, Phys. Lett.B **571** (2003) 45, `https://doi.org/10.1016/j.physletb.2003.08.014`.
16. A. H. Al-Ghamdi, Awad A. Ibraheem,and M.El-Azab Farid,*An investigation of* ^{4}*He+* ^{12}*C and* ^{4}*He+* ^{16}*O reactions using the cluster model*, Commun. Theor. Phys. **581** (2012) 135, `https://doi.org/10.1088/0253-6102/58/1/17`.
17. P. P. Manngrd *et al.*,*Molecular potential and elastic scattering of alpha particles by* ^{28}*Si from 14 to 28 MeV*, Nucl. Phys. A **504** (1989) 130, `https://doi.org/10.1016/0375-9474(89)90286-8`.
18. M. M. Billah *et al.*, *Alpha – Ni optical model potentials*, Nucl. Phys. A **762** (2005) 50, `https://doi.org/10.1016/j.nuclphysa.2005.07.020`.
19. A. S. B. Tariq *et al.*,*Potential description of anomalous large angle scattering of alpha particles*, Phys.Rev.C **59** (1999) 2558, `https://doi.org/10.1103/PhysRevC.59.2558`.
20. S. Hossain *et al.*, *Non-monotonic potential description of alpha – Zr refractive elastic scattering*, J. Phys. G: Nucl. Part. Phys. **40** (2013) 105109, `https://doi.org/10.1088/0954-3899/40/10/105109`.
21. M. S. Islam, M. M. Billah and A. K. Basak, *Non-monotonic potential description of alpha-*^{40}*Ca refractive elastic scattering*, J. Phys.: Conf. Ser. **1718** (2021) 012008, `https://doi.org/10.1088/1742-6596/1718/1/012008`.
22. S.Adachi *et al.*,*Systematic analysis of inelastic* α *scattering off self-conjugate A= 4 n nuclei*, Phys.Rev.C **97** (2018) 014601, `https://doi.org/10.1103/PhysRevC.97.014601`.
23. H. Abele *et al.*,*Measurement and folding-potential analysis of the elastic* α*-scattering on light nuclei*, Zeitschrift fÃ$\frac{1}{4}$r Physik A Atomic Nuclei **326** (1987) 373, `https://doi.org/10.1007/BF01289540`.
24. H. Abele and G. Staudt,α- ^{16}*O and* α-^{15}*N optical potentials in the range between 0 and 150 MeV*, Phys. Rev. C **47** (1993) 742, `https://doi.org/10.1103/PhysRevC.47.742`.
25. D. T. Khoa, G. R. Satchler, W. von Oertzen, *Nuclear incompressibility and density dependent interactions in the folding model for nucleus-nucleus potentials*, Phys. Rev. C **56** (1997) 954, `https://doi.org/10.1103/PhysRevC.56.954`.
26. M. EL-Azab Farid, Z. M. M. Mahmoud, and G. S. Hassan, *Analysis of heavy ions elastic scattering using the double folding cluster model*, Nucl. Phys. A **691** (2001) 671, `https://doi.org/10.1016/S0375-9474(01)00587-5`.
27. T. Furumoto and Y. Sakuragi, *Application of the Jeukenne-Lejeune-Mahaux folding model to* α*-nucleus elastic scattering*, Phys. Rev. C **74** (2006) 034606, `https://doi.org/10.1103/PhysRevC.74.034606`.
28. K. O. Behairy, Z. M. M. Mahmoud, M. Anwar, α*-particle elastic scattering from 12C, 16O, 24Mg, and 28Si*, Nucl. Phys. A 957 (2017) 332, `https://doi.org/10.1016/j.nuclphysa.2016.09.008`.
29. Z. M. M. Mahmoud and K. O. Behairy,α*-Cluster Optical Potential Model of* ^{40}*Ca*, Braz. J. Phys. **47** (2017) 189, `https://doi.org/10.1007/s13538-016-0483-7`.
30. Awad A. Ibraheem and M. Aygun, *Optical model analysis of alpha particle scattering*, Indian J. Phys. **95**, (2021) 2437, `https://doi.org/10.1007/s12648-020-01903-3`.
31. M. N. A. Abdullah *et al.*, *Cluster structure of* ^{16}*O*, Eur. Phys. J. A **18** (2003) 65, `https://doi.org/10.1140/epja/i2002-10168-7`.
32. M. A. Hassanain, *Cluster Folding Model Analysis of* α*-Particle Elastic Scattering by* ^{24}*Mg and* ^{28}*Si*, Chin.J.Phys. **49** (2011) 589,
33. Z. M. M. Mahmoud,*Energy density functional for* α *clustering and scattering of light A= 4 m nuclei*, Phys. Rev. C **105** (2022) 044609, `https://doi.org/10.1103/PhysRevC.105.044609`.
34. Z. M. M. Mahmoud *et al.*,*Analysis of alpha scattering from* α*-conjugate nuclei*, J.Phys.Soc. Japan **88** (2019) 024201, `https://doi.org/10.7566/JPSJ.88.024201`.
35. I. Reichstein, F. B. Malik, *Dependence of* ^{16}*O*-^{16}*O potential on the density ansatz*, Phys. Lett. B **37** (1971) 344, `https://doi.org/10.1016/0370-2693(71)90197-3`.
36. I. Reichstein, F. B. Malik, Potential energy surfaces and lifetimes for spontaneous fission of heavy and superheavy elements from a variable density dependent mass formula, Ann. of Phys. **98** (1976) 322, `https://doi.org/10.1016/0003-4916(76)90157-3`.
37. I. Reichstein and F. B. Malik, *Condensed matter theories* **1** (1985) 291.
38. `http://nrv.jinr.ru/nrv/webnrv/map/`.
39. M. Karakoç, BiFold:*A Python code for the calculation of double-folded (bifold) potentials with density-in/dependent nucleon-nucleon interactions*, Comput. Phys. Comm. **284** (2023) 108613, `https://doi.org/10.1016/j.cpc.2022.108613`.
40. J. Cook ,*DFPOT-a program for the calculation of double folded potentials*, Comput. Phys. Comm.**25** (1982) 125, `https://doi.org/10.1016/0010-4655(82)90029-7`.
41. B. Buck, H. Friedrich and C. Wheathly, *Local potential models for the scattering of complex nuclei*, Nucl. Phys. A **275** (1977) 246, `https://doi.org/10.1016/0375-9474(77)90287-1`.
42. N. M. Clarke, *HI-OPTIM code* (1994), University of Birmingham, UK (unpublished).
43. Sh. Hamada, Awad. A. Ibraheem, *Comparative Analysis for* ^{6}*Li +* ^{58}*Ni System Within the Framework of Various Nuclear Potentials*, Braz.J.Phys. **29** (2022) 52, `https://doi.org/10.1007/s13538-021-01035-x`.
44. I. J. Thompson,*Coupled reaction channels calculations in nuclear physics*, Comput. Phys. Rep. **7** (1988) 167, `https://doi.org/10.1016/0167-7977(88)90005-6`.
45. S. M. Smith *et al.*,*The and* α*,* ^{3}*He) reactions on* ^{12}*C at 139 MeV*, Nucl. Phys. A **207** (1973) 273, `https://doi.org/10.1016/0375-9474(73)90347-3`.
46. M. E. Brandan and K. W. McVoy, *Rainbow-shift mechanism behind discrete optical-potential ambiguities*, Phys. Rev. C **43** (1991) 1140, `https://doi.org/10.1103/PhysRevC.43.1140`.

47. A. Kiss *et al.*,*Inelastic scattering of 172.5 MeV α particles by ^{12}C*, J. Phys. G: Nucl. Phys. **13**, (1987) 1067, `https://doi.org/10.1088/0305-4616/13/8/014`.

48. K. T. Knopfle *et al*.,*Evidence for the Isoscalar Giant Quadrupole Resonance in ^{16}O*, Phys.Rev. Lett. **35**(12) (1975) 779, `https://doi.org/10.1103/PhysRevLett.35.779`.

49. K. Van der Borg, M. N. Harakeh and A. Van der Woude, *The isoscalar strength distribution in $^{24,26}Mg$, ^{28}Si and ^{40}Ca obtained from inelastic alpha scattering at 120 MeV*, Nucl. Phys. A **365** (1981) 243, `https://doi.org/10.1016/0375-9474(81)90297-9`.

50. D. Arani Sarker, M. D. A. Rahman and H. M. Sen Gupta, *A study of scattering of alpha particles from nuclei*, Int. J. of Mod. Phys. E, **19** (11) (2010) 2167,`https://doi.org/10.1142/S0218301310016570`.

51. Y. Kanada-Enyo, K. Ogata,*Transition properties of low-lying states in ^{28}Si probed via inelastic proton and α-scattering*, Phys. Rev. C **101** (2020) 064607 `https://doi.org/10.1103/PhysRevC.101.064607`.

52. Y. Kanada-Enyo, K. Ogata,*First microscopic coupled-channels calculation of cross sections for inelastic α scattering off ^{16}O*, Phys. Rev. C **99** (2019) 064608. `https://doi.org/10.1103/PhysRevC.99.064608`.